Ultrasonics - Sonochemistry 56 (2019) 134–142

Contents lists available at ScienceDirect

Ultrasonics - Sonochemistry

journal homepage: www.elsevier.com/locate/ultson

Ultrasound-assisted synthesis of tungsten trioxide entrapped with graphene nanosheets for developing nanomolar electrochemical (hormone) sensor and enhanced sensitivity of the catalytic performance

Mani Govindasamy[a], Bowya Subramanian[b,c], Sea-Fue Wang[a,*], Sathishkumar Chinnapaiyan[d], R. Jothi Ramalingam[e,*], Hamad A. Al-lohedan[e]

[a] Department of Materials and Mineral Resources Engineering, National Taipei University of Technology, No. 1, Sec. 3, Chung-Hsiao East Rd., Taipei 106, Taiwan
[b] Department of Information Technology, KSR College of Engineering, Tiruchengode, Tamil Nadu, India
[c] Department of Electrical Engineering and Computer Science, National Taipei University of Technology, No. 1, Sec. 3, Chung-Hsiao East Rd., Taipei 106, Taiwan
[d] International Master Program in Mechanical and Automation Engineering, National Taipei University of Technology, No. 1, Section 3, Chung-Hsiao East Road, Taipei 106, Taiwan
[e] Surfactant Research Chair, Chemistry Department, College of Science, King Saud University, P.O. Box-2455, Riyadh 11451, Saudi Arabia

ARTICLE INFO

Keywords:
Tungsten trioxide
Sonochemical synthesis
Biomarker
Graphene
Biological samples

ABSTRACT

Herein, we have reported a simple sonochemical synthesis of multi-layer graphene covered tungsten trioxide nanoballs (WO_3 NBs) and the nanocomposite was characterized by FESEM, HRTEM, XRD, XPS, CV and EIS. Furthermore, progesterone (PGT) is a preferred marker for various biological problems like pregnancy problem, mood swings, anxiety, depression, nervousness and body pain. Therefore, its selective and sensitive determination in various biological fluids is beneficial for the evaluation of malformation problems. We describe the fabrication of an amperometric and non-enzymatic biosensor based on WO_3 NBs@GR nanocomposite modified electrode for nanomolar detection of PGT. The results showed that the nanocomposite modified electrode exhibit well-defined electro-oxidation peak compared to bare and control electrodes, demonstrating the superior electrocatalytic ability and performances. The fabricated modified sensor was facilitates the analysis of PGT in the concentration ranges of 0.025–1792.5 μM with a low detection limit of 4.28 nM. Further, the as-prepared WO_3 NBs@GR electrode has been applied to determination of PGT in human blood samples with outstanding recovery results and more importantly, the facile and environment-friendly sonochemical construction strategy extended here, may be open a cost-effective way for setting up the nanocomposites based (bio) sensing platform.

1. Introduction

Progesterone (PGT) are important hormone and it is endogenous-steroid and female sex hormone involved in the pregnancy, menstrual cycle and embryogenesis of humans [1–3]. Furthermore, PGT is an important signal biomolecule for various biological and chemical processes. Studies on the electro-chemistry of PGT is significant as it regulates biological functions and play significant role in women health [2,4]. PGT is level ranges from 11.2 to 90 ng/mL in blood serum for pregnant women and the menstrual cycle level range is 5–20 ng/mL [5,6]. An abnormal concentration level is an indication of several problem such as pregnancy problem, mood swings, anxiety, depression, nervousness, body pain and etc [7–10]. Therefore, a sensitive and rapid detection in low concentrations in biological fluids are becoming more and more important. Hence, various detection methods including such as radioimmunoassay (RIA), gas-high performance liquid chromatography (HPLC) [11], enzyme-linked immunosorbent assay (ELISA) [2], fluorescence-based screening assay (FSA) and micellar electrokinetic chromatography [12]. However, most of these methods are tedious protocols, time consuming, and more expensive [13–18]. On the contrary, the electrochemical method is simple and rapid current response with high sensitivity.

Trioxide based transition metal oxides (TMO) have received much attention due to their excellent physicochemical properties which are suitable for electrocatalysis, batteries, hydrogen and oxygen evaluations, electrochemical sensor and biosensors [19–22]. Moreover, the tungsten trioxide (WO_3) nanoparticles are well known for their interesting electronic and electrocatalytic properties and efficient way to improve the performances in energy and sensing applications [23–26]. Furthermore, this work we have synthesized the WO_3 NBs catalyst by a

* Corresponding authors.
E-mail addresses: sfwang@ntut.edu.tw (S.-F. Wang), jrajabathar@ksu.edu.sa (R. Jothi Ramalingam).

https://doi.org/10.1016/j.ultsonch.2019.03.021
Received 1 March 2019; Received in revised form 21 March 2019; Accepted 21 March 2019
Available online 21 March 2019
1350-4177/

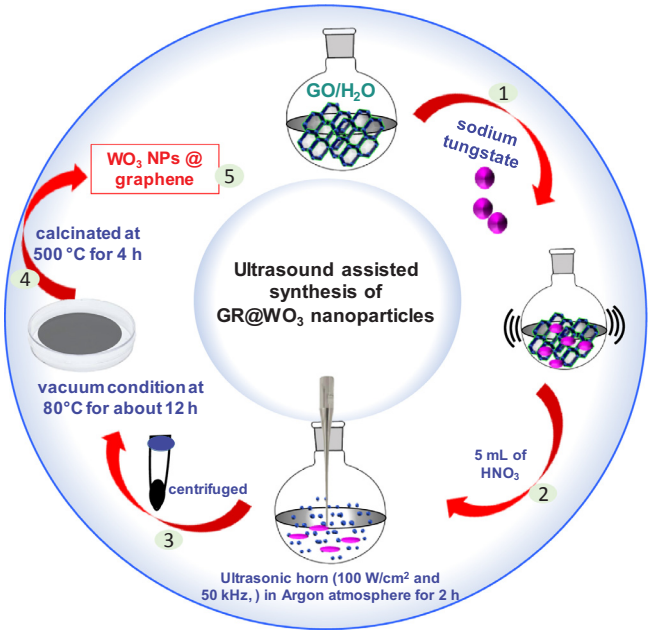

Scheme 1. Sonochemical synthesis of nanocomposite.

simple sonochemical reduction approach. Therefore, this studies report that the trioxide based electrocatalyst amplify the electrocatalytic response towards hormone detection.

Furthermore, graphene (GR) is a two-dimensional layered nanosheets and its interesting physicochemical properties such as high electrical conductive and large surface area [27–32]. Moreover, owing to their significant electrocatalytic properties of GR is provide a numerous prospect into the energy and (bio) sensing applications [33–35]. Nonetheless, WO_3 NBs based carbonaceous nanomaterials that are exhibited the excellent electrochemical properties [36–38]. Because, the presence of GR can enhance the electrocatalytic ability of the nanocomposite and the GR is essential for improving the electrochemical surface area of nanocomposite [39–41]. In this studies, the synthesized WO_3 NBs were combine with GR using a simple and facile sonochemical approach (Scheme 1). In the present work, the synthesized WO_3 NBs@GR nanocomposite modified electrode was fabricated by a drop-casted strategy. After the fabrication, the synthesized WO_3 NBs@GR nanomaterial was used to determination of endogenous-steroid. We achieved, the high sensitivity and excellent practical ability were analyzed using by voltammetry and amperometric techniques (Scheme 2). To the best our knowledge, this modified sensor has achieved a lowest LOD (limit of detection).

2. Experimental section

2.1. Synthesis of WO_3 NBs@GR nanocomposite

All reagents and chemicals were collected from Sigma-Aldrich and used without any other purifications (chemicals and methods detail are given in Supporting information file). A typical synthesized 20 mg of graphene oxide were subsequently added to the pre-prepared mixture solution of sodium tungstate in 50 mL of deionized water. Then, 5 mL HNO_3 was added under the stirring and then ultrasonicated for 15 min. After the suspension was sonicated in ultrasonic bath of 100 W at 50 kHz for 2 h. Finally, WO_3 NBs@GR nanocomposite was obtained by filtrating and drying at 80 °C for 12 h (Scheme 1). For controlled experiments, pure WO_3 NBs and GR were also prepared using the procedure described above but without an addition of graphene oxide and sodium tungstate respectively.

2.2. Fabrication of WO_3 NBs@GR modified electrode

The WO_3 NBs@GR nanomaterials dispersed solution (3 mg/mL; ethanol/water; 50/50%) about 3 µL was drop-casted (three times) on the pre-cleaned electrode surface. Finally, the WO_3 NBs@GR modified electrode was dried at room temperature. Furthermore, same produce was applied to fabricate the control electrodes such as GR and WO_3 NBs. Then, the modified electrode was applied for the electrochemical determination of the PGT.

3. Results and discussion

3.1. Surface morphological analysis

FESEM image of reduced graphene nanosheets shown in Fig. 1A. Its paper like layered multi-carbon sheets and WO_3 NBs are given in Fig. 1B–C. The surface morphology of the as-synthesized reduced graphene nanosheets wrapped WO_3 NBs nanoparticles was scrutinized by HRTEM and the corresponding images were presented in Fig. 1D–F. As HRTEM shows the nanoballs like structure was observed for the synthesized WO_3 NBs nanoparticles with (Sonochemically reduced) GR. These results are confirmed that the formation of WO_3 NBs@GR nanocomposite.

3.2. XRD and XPS analysis

The XRD patterns of GR, WO_3 NBs and WO_3 NBs@GR was displayed in Fig. 2. The XRD pattern of the WO_3 NBs@GR shows, several diffraction peaks are observed that are correlated to cubic plane and this diffraction patterns are matched with the cubic phase of WO_3 NBs (JCPDS No. 20-1324) [42–44]. Therefore, the XRD pattern indicates the successful formation of WO_3 NBs. Besides, the GR exhibited the diffraction peaks assigned for the miller indices plane is (0 0 2) [45]. Furthermore, formation of WO_3 NBs are evaluated by XRD (Fig. 2). Finally, these information are regenerated in the WO_3 NBs@GR confirms the composite formation.

X-ray photoelectron spectroscopy (XPS) is one of the specific tool for the evaluation of the oxidation states in the nanocomposites. Fig. 3A demonstrates the XPS survey spectra of the WO_3 NBs@GR. As can be seen that the characteristic peaks for C 1s, O 1s and W 4f levels were observed at their correlated binding energies [46,47]. As shown in Fig. 3B, the high resolutions scan of the C 1s represents the major peak due to ring carbon [48]. In Fig. 3C, two dominant peaks of W 4f bounded with the metals that exhibited the W $4f_{7/2}$ and W $4f_{5/2}$ located at the (35.4 eV) and (37.5 eV). Furthermore, the XPS spectrum of the O 1s present in the WO_3 reveals the primary peak denotes the W-O bond located at 530.7 eV (Fig. 3D), which demonstrate the oxygen present in the form of bridging with tungsten atom [49–51]. The XPS results confirms existence of all elements in the WO_3 NBs@GR nanocomposite [52,53].

3.3. Electrochemical behavior of modified electrodes

The interfacial electron transport behavior of the electrocatalyst modified electrodes were studied using EIS (electrochemical impedance spectroscopy). The Nyquist plot is at WO_3 NBs/GCE (a), GR/GCE (b) and WO_3 NBs@GR/GCE (c) shown in (Fig. 4A). The EIS analysis were carried out by 0.1 M KCl containing 5 mM $[Fe(CN)_6]^{-3/-4}$ electrolyte solution (frequency range = 100 MHz–100 kHz). For the comparison, the GR/GCE and WO_3 NBs/GCE depicts the higher semicircular and larger R_{ct} value around 587.43 Ω and 243.31 Ω than WO_3 NBs@GR/GCE. Furthermore, the WO_3 NBs/GR nanocomposite shows the lowest R_{ct} value of 128.56 Ω. Therefore, the nanocomposite has good conductivity and excellent catalytic ability.

Furthermore, the interfacial electron transport behavior was analyzed using cyclic voltammetry (CV) method. The CV analysis was

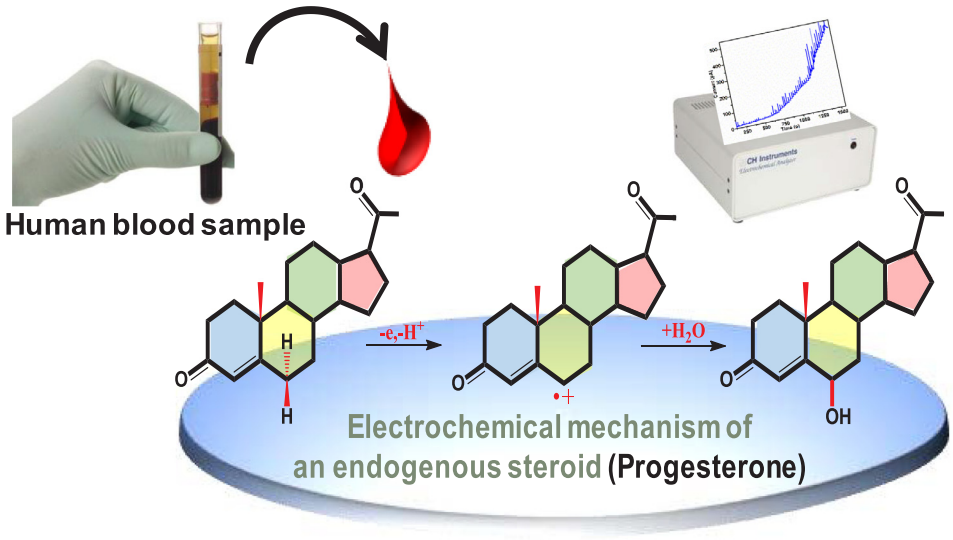

Scheme 2. The electrochemical oxidation mechanism of PGT based on WO_3 NBs@GR/GCE.

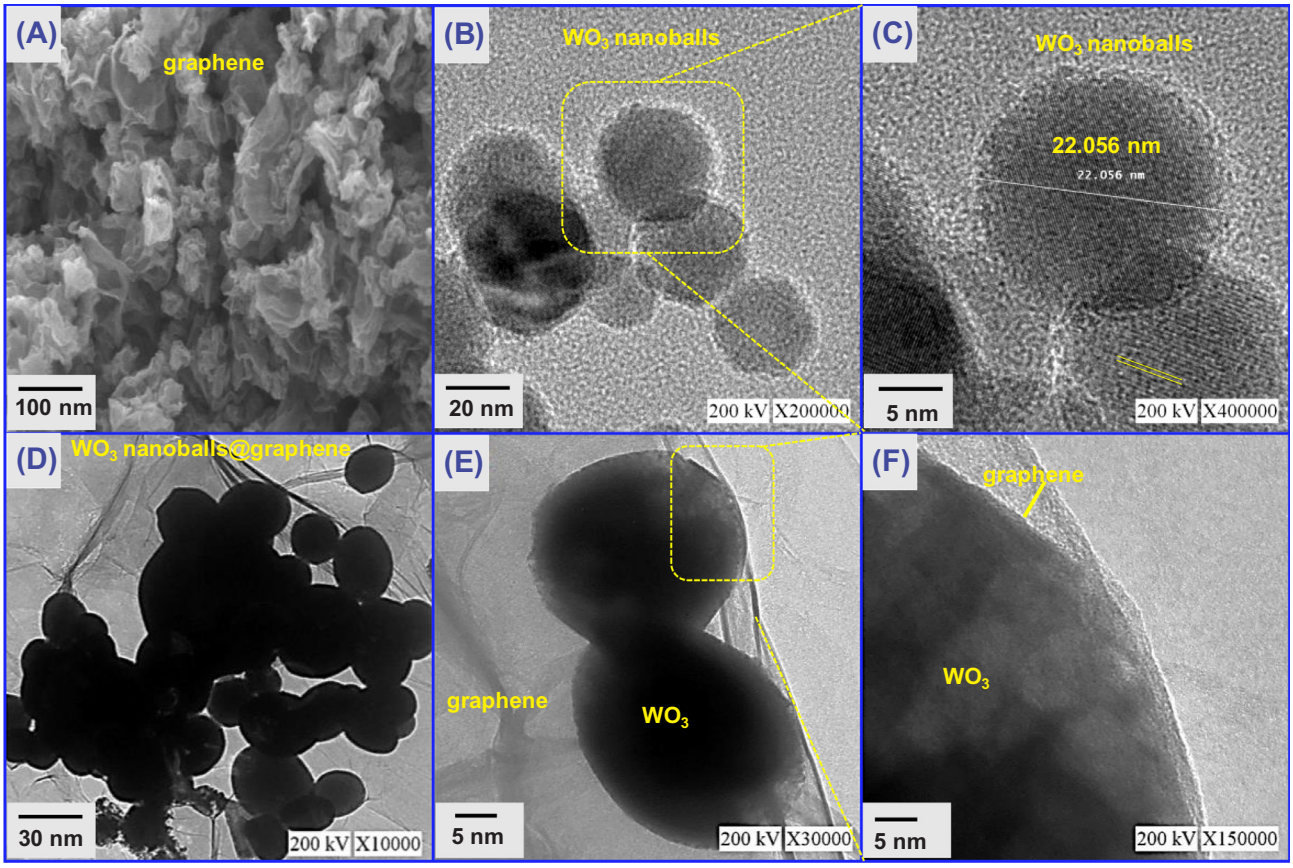

Fig. 1. FESEM images of GR (A). HRTEM images of WO_3 NBs (B–C), WO_3 NBs@GR nanocomposite (D) and high magnification images (E–F).

carried out by 0.1 M KCl containing 5 mM $[Fe(CN)_6]^{-3/-4}$ solution at a fixed scan rate of 50 mVs^{-1}. Fig. 4B depicts the CVs of modified electrodes including bare GCE (a), GR/GCE (b), WO_3 NBs/GCE (c) and WO_3 NBs@GR/GCE (d). The nanocomposite has high peak current compared with other control electrodes such as bare GCE, GR/GCE, and WO_3 NBs/GCE. Fig. 4C, shows that the scan rate of the WO_3 NBs@GR modified electrode. Fig. 4D, is corresponding calibration plot of the scan rate (20 mVs^{-1} to 300 mVs^{-1}). In addition, using the randles sevcik equation (1) the electrochemical active surface area of WO_3 NBs/GCE, GR/GCE, and WO_3 NBs@GR/GCE were calculated to be 0.121, 0.148 and 0.174 cm^2 respectively. Therefore, the WO_3 NBs@GR nanocomposite modified GCE exhibit the higher surface area and good catalytic activity.

$$I_p = 2.69 \times 10^5 n^{3/2} A D^{1/2} C v^{1/2}$$

3.4. Electro-oxidation of PGT on WO_3 NBs@GR/GCE

The electrochemical behavior of the PGT was investigated at modified and unmodified electrodes by CV method. Fig. 5A exhibited the CV

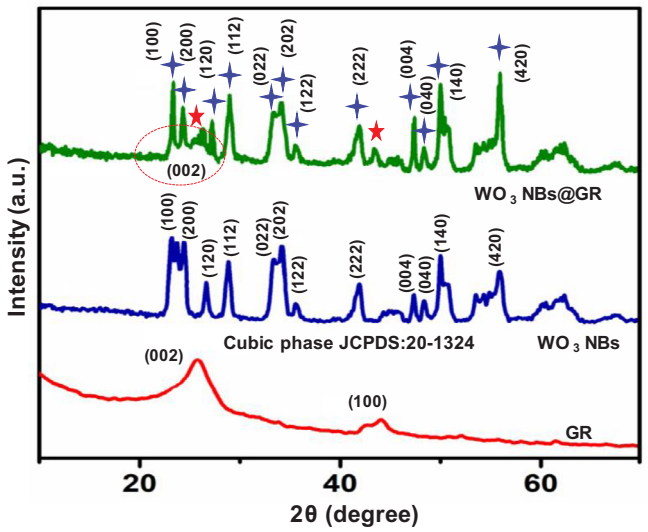

Fig. 2. XRD analysis of GR, WO_3 NBs, and WO_3 NBs@GR nanocomposite.

curves of the bare GCE (a), GR/GCE (b), WO_3 NBs/GCE (c) and WO_3 NBs@GR/GCE (d) for the addition of (100 μM) PGT in 0.05 M PB (pH 7.0). The bare GCE oxidation of PGT is low peak current value (3.12 μA). Moreover, the GCE was modified with GR and WO_3 NBs, the oxidation peak current was increased. Fascinating, the excellent anodic peak current (32.5 μA) and lowest overpotential at 0.31 V was obtained at WO_3 NBs@GR nanocomposite modified GCE (Fig. 5B). Therefore, the electrochemical performance towards PGT oxidation is improved due to the synergistic effect of the GR nanosheets and WO_3 NBs. Moreover, the electrochemical oxidation mechanism of PGT is given in Scheme 2.

Furthermore, the electrocatalytic ability of the nanocomposite was analyzed towards the PGT oxidation by adding the various concentrations in 0.05 M PB. As shown in Fig. 5C, the anodic peak currents were increased linearly for the increasing concentration PGT from 25 to 125 μM. In addition, the oxidation linear regression equation $y = -0.2195x - 12.714$ with the correlation co-efficient of $R^2 = 0.9937$ (Fig. 5D). Therefore, these results are valuable evidences for the excellent electrochemical performance of PGT on the WO_3 NBs@GR/GCE.

The effect of the different scan rates on WO_3 NBs@GR/GCE in the presence of 100 μM PGT was displayed in Fig. 6A. Moreover, the anodic peak currents were increase with the increasing of scan rates from 20 to 200 mV/s. Moreover, the obtained anodic peak currents are plotted against the square root of the scan rates. In Fig. 6B, anodic peak currents were linearly proportional to the square root of the scan rates and the correlation coefficient of $R^2 = 0.9972$ was observed. These results clearly indicate that the electro-oxidation of PGT at WO_3 NBs@GR/GCE is diffusion controlled process.

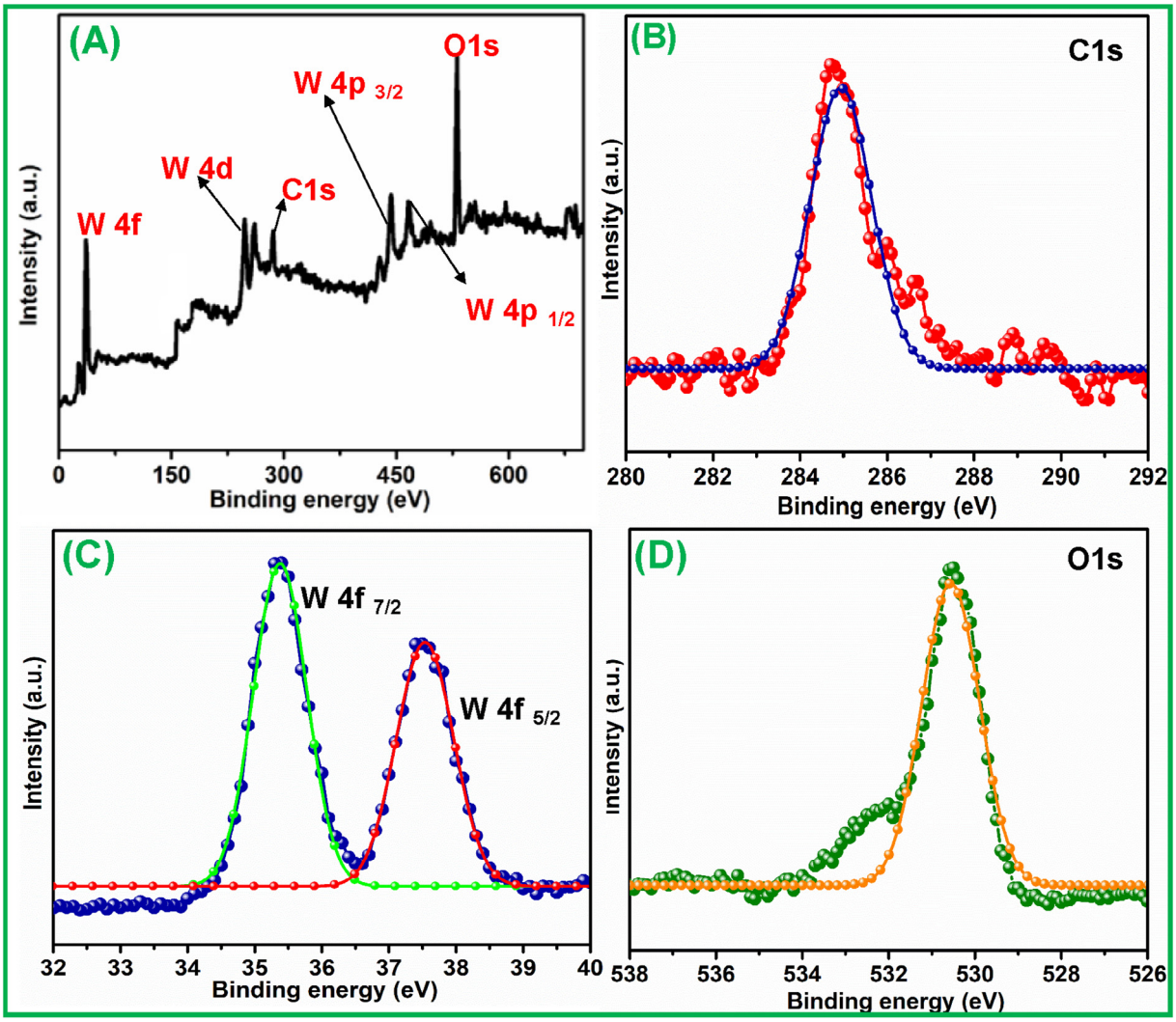

Fig. 3. XPS survey spectrum of WO_3 NBs@GR (A) and de-conventional peaks of C1s (B), W 4f (C) and O 1s (D).

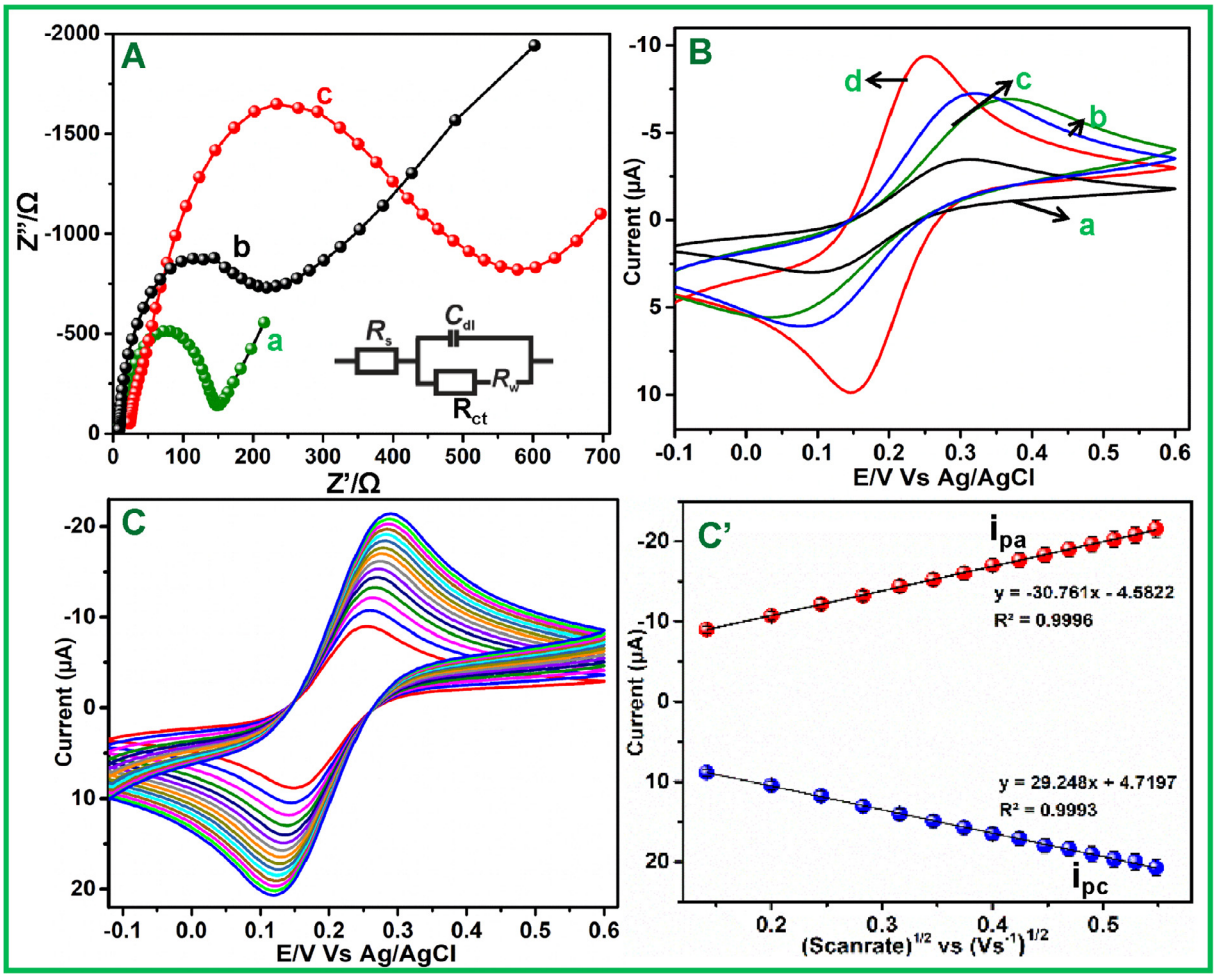

Fig. 4. (A) EIS spectra of WO_3 NBs/GCE (a), GR/GCE (b), and WO_3 NBs@GR/GCE (c). (B) CVs of bare GCE (a), GR/GCE (b), WO_3 NBs/GCE (c) and WO_3 NBs@GR/GCE (d) in 0.1 M KCl containing 5 mM $[Fe(CN)_6]^{-3/-4}$ and Randles equivalent circuit model (inset). (C) Scan rate of the nanocomposite modified electrode and (D) Calibration plot of (scan rate)$^{1/2}$ vs $(mVs^{-1})^{1/2}$.

In Fig. 6C, shows the CV plot of different pH 3.0 to pH 11.0 in presence of 100 μM PGT at WO_3 NBs@GR/GCE. It can be seen that the anodic peak current response was increased form pH 3.0 to pH 7.0, then it gradually decreases from pH 7.0 to pH 11.0. Moreover, the faradic process which involves the deprotonation during the electro-oxidation of PGT that facilitated at the higher pH values. The obtained anodic peak current values are plotted against the different pH in Fig. 6C. According to the results, the maximum electro-catalytic response of PGT at the WO_3 NBs@GR/GCE was obtained at pH 7.0. Therefore, we chose this pH 7.0 for all the electrochemical detection experiments.

3.5. Electrochemical determination of PGT by amperometric technique on WO_3 NBs@GR

The amperometric technique is one of the important technique for the quantitative determination of analysis. Fig. 7A, shows the amperometric *i-t* response of WO_3 NBs@GR nanocomposite film modified rotating disc GCE upon various addition of PGT into continuously stirred PB (pH 7.0) at the rotation speed of 1200 rpm and constant applied potential is +0.21 V. Fig. 7A, shows the amperometric for the determination of PGT for the different concentrations additions from 0.025 to 1792.5 μM and Fig. 7A (inset) depicts the amperometric peaks of the lower concentration of PGT. Mainly, the electrocatalytic peak current response was increased for each addition of PGT. Moreover, the obtained peak current values were plotted against the different concentrations of PGT and the results are displayed in Fig. 7B. Furthermore, the linear regression equation of PGT is $y = 0.293x + 0.969$ with the correlation coefficient $R^2 = 0.9998$. Therefore, the peak current responses were increased linearly proportional to the different concentration of PGT. According to the results, the sensor linear range is 0.025–1792.5 μM. The sensitivity of the sensor was estimated to be 3. 708 μA μM^{-1} cm^{-2} and the limit of detection (LOD = $3s_b/S$, s_b = standard deviation of blank signal and S = sensitivity) was calculated to be 4.28 nM. Notably, the modified sensor was achieved very low detection limit compared with previous literature. In the comparison, the amperometric technique was exhibited the good linear range and excellent LOD [2,3]. These results confirm that the outstanding electrocatalytic performance of the WO_3 NBs@GR modified electrode towards PGT.

3.6. Selectivity, stability, reproducibility and repeatability of the sensor

In order to investigate the biologically important molecules on the WO_3 NBs@GR modified electrode. Fig. 8A. exhibited the amperometric responses for the additions of 0.5 mM of H_2O_2, folic acid (FA), uric acid (UA), glucose (Glu), NO_2^-, Tyrosine (TS), dopamine (DA), serotonin (ST), vanillin (VI) and ascorbic acid (AA) in presence of 50 μM of PGT. Furthermore, the obtained amperometric responses reveal that other biological molecules are not affects much of the PGT response. Therefore, these results are explaining the good selectivity based on the WO_3 NBs@GR/GCE towards PGT detection.

The nanocomposite fabricated sensor retained 96.12% of its initial

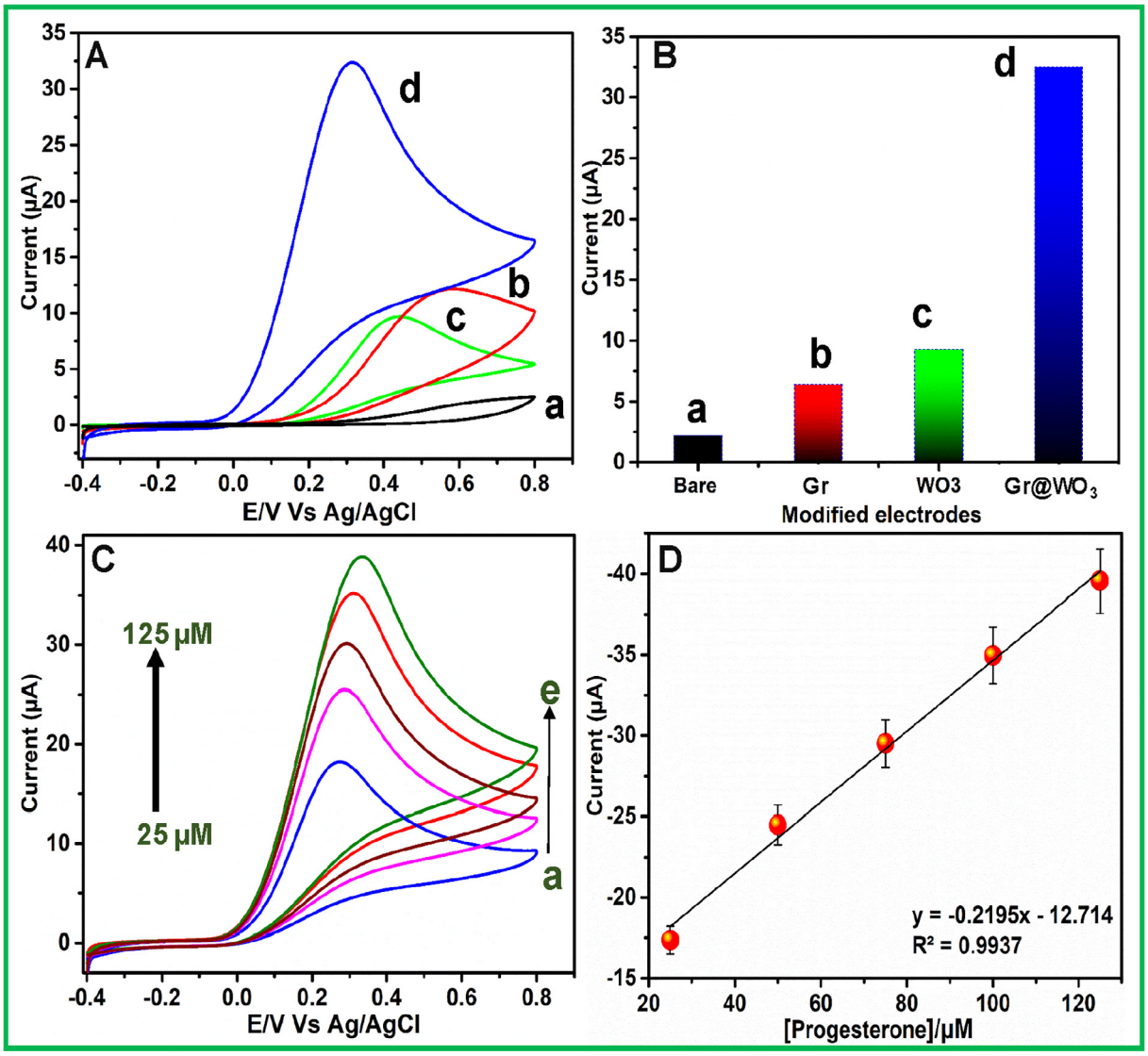

Fig. 5. (A) CVs of bare GCE (a), GR/GCE (b), WO_3 NBs/GCE (c) and WO_3 NBs@GR/GCE (d) containing 100 μM PGT in 0.05 M PB at the scan rate at 50 mV/s. (C) Increasing concentration of PGT (25–125 μM) in 0.05 M PB (pH 7.0) at WO_3 NBs@GR/GCE. (D) the calibration plot between [PGT]/μM vs anodic peak currents.

response current after 45 days of its storage (WO_3 NBs@GR/GCE) validating the appreciable storage stability. For the reproducibility analysis ten different WO_3 NBs@GR/GCE were prepared and the amperometric response were recorded in presence of 100 μM of PGT. The obtained results were given in Fig. S1 and the relative standard deviation (RSD) value were calculated to be 3.21%. The WO_3 NBs@GR/GCE was tested for eight times and the RSD value were calculated to be 3.52% (Fig. S2). As a results, WO_3 NBs@GR/GCE shows the excellent selectivity, stability and reproducibility towards the detection of PGT.

3.7. Real sample analysis

The practical feasibility of the WO_3 NBs@GR/GCE modified electrode was investigated. First, the human serum samples were diluted with buffer and spiked with a specified concentration of PGT by using the standard addition method. Later, the samples were used to explore the practicality of the proposed sensor. Amperometric responses for the addition of human serum samples spiked with 100–500 nM concentration of PGT. Hence, the peak current responses were increased for each addition of PGT spiked samples (Fig. S3). The obtained peak current responses have calculated against the concentration. Moreover, the RSD (n = 3) results were calculated and tabulated in Table 1. It can be seen that the appreciable recovery results were obtained for the determination of PGT in human serum samples Table 1. These results clearly reveal that the practical feasibility of the proposed sensor.

4. Conclusion

In summary, we synthesized the WO_3 NBs decorated graphene nanocomposite through simple and facile sonochemical method. Moreover, the nanomaterial was characterized through the appropriate spectrophotometric techniques such as FESEM, HRTEM, XRD, XPS, EIS and electrochemical method. As-prepared WO_3 NBs@GR nanocomposite was used to fabricate the modified GCE for the determination PGT. The electrocatalytic activity of the WO_3 NBs@GR/GCE for the detection of PGT was evaluated by CV and amperometric methods. Furthermore, the amperometric analysis reveals the wide linear range 0.025–1792.5 μM and nanomolar LOD (4.28 nM) towards PGT. Additionally, proposed sensor has exhibited a good selectivity, stability and reproducibility. Furthermore, the practical feasibility of the PGT sensor was demonstrated in human blood samples.

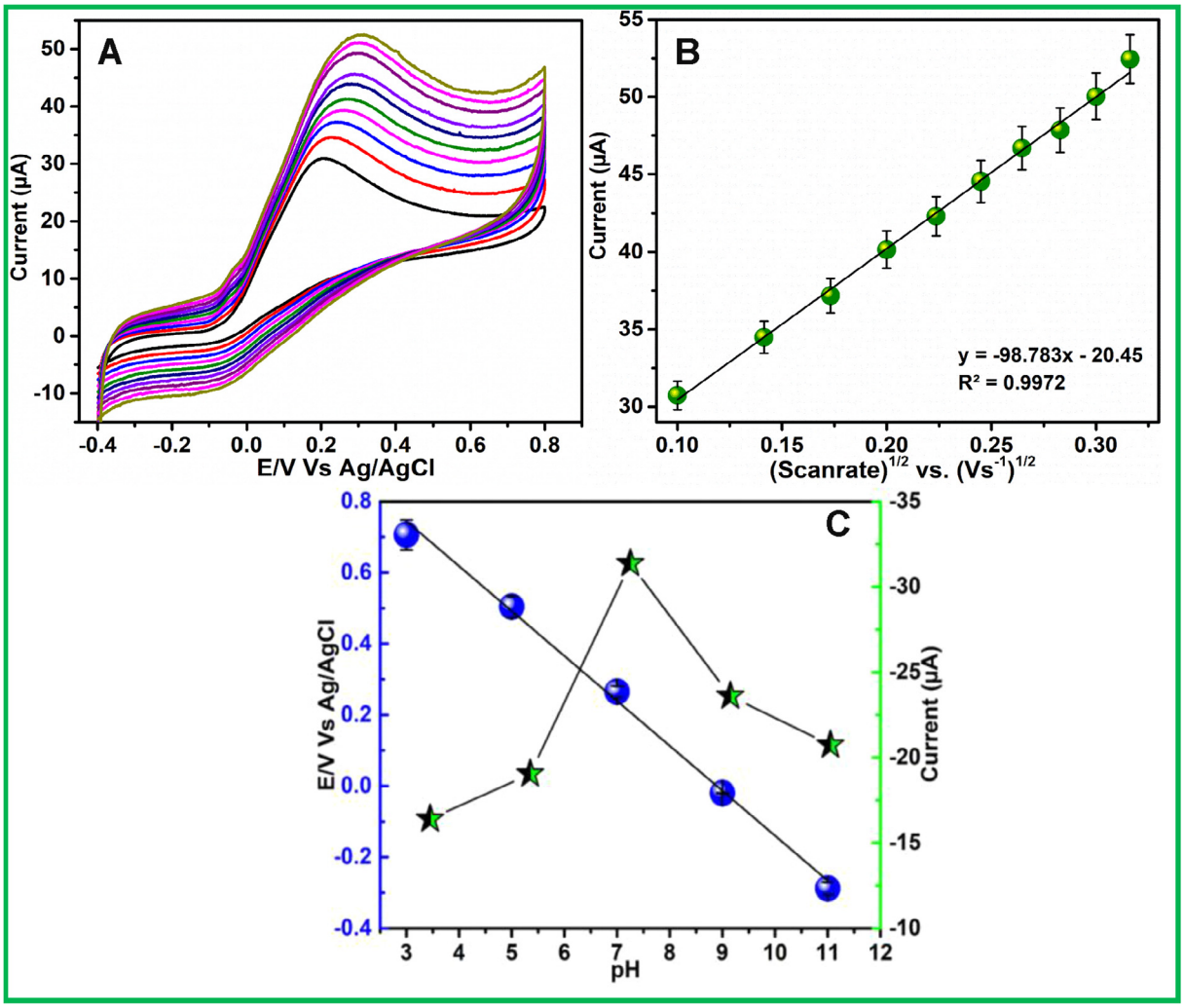

Fig. 6. (A) CV curves of different scan rates from (20 to 200 mV/s) on WO_3 NBs@GR/GCE for the oxidation of 100 μM PGT in 0.05 M PB. (B) The calibration plot between the anodic peak current (I_{pa}) against the square root of the scan rates. (C) CVs of the WO_3 NBs@GR/GCE in the presence of 100 μM PGT in various pH solutions and plot of pH vs anodic peak current (I_{pa}/μA) with different pH vs peak potential (E_{pa}/V).

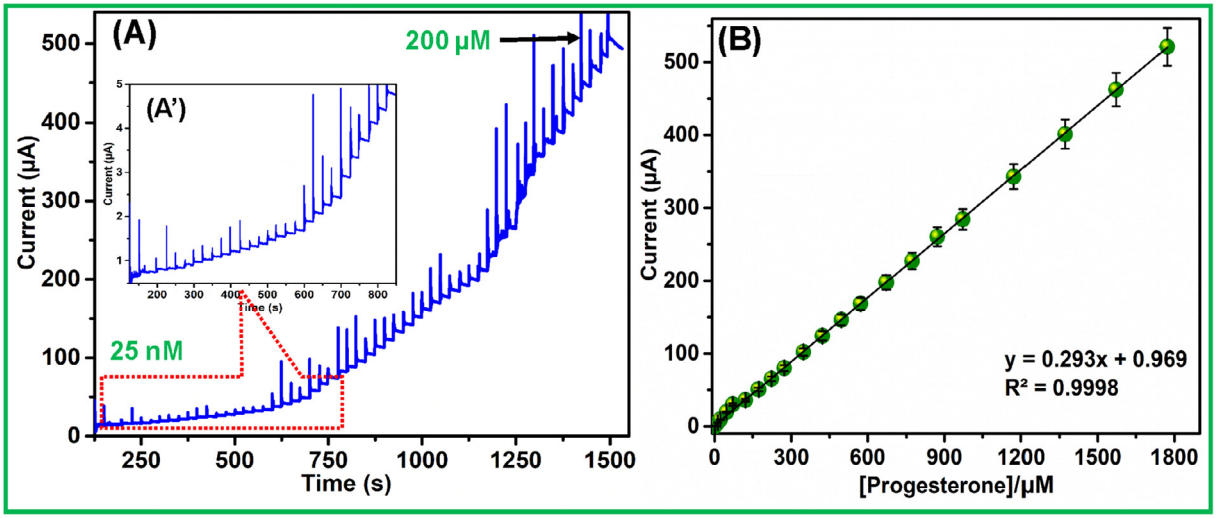

Fig. 7. (A) Amperometric responses for the successive additions of PGT in 0.05 M PB (pH 7.0) and various concentration ranges from (0.025 to 1792.5 μM) at WO_3 NBs@GR/GCE. (B) The linear plot of PGT concentrations versus current response.

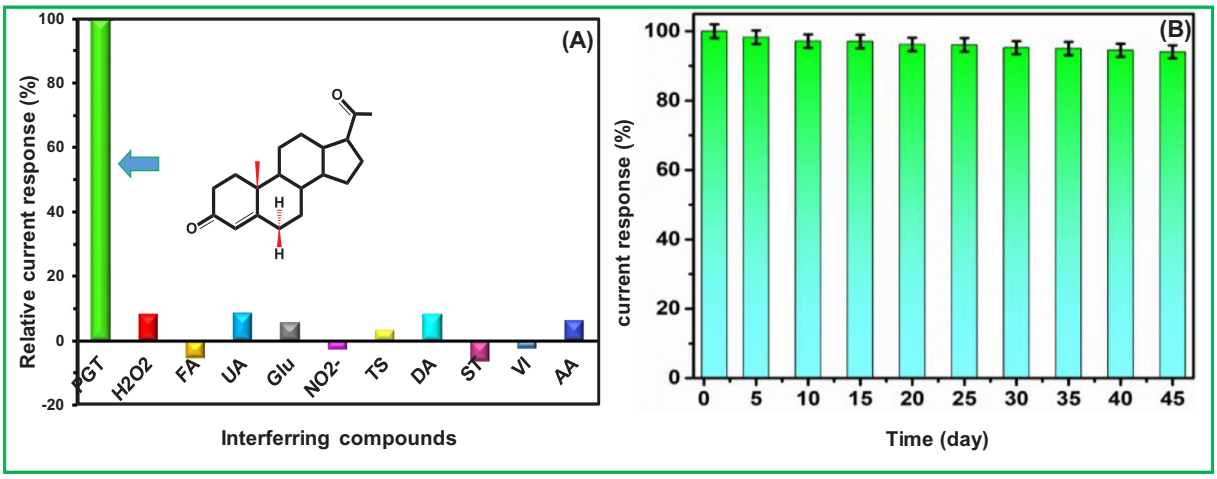

Fig. 8. (A) Amperometric selective responses of WO_3 NBs@GR/GCE towards 50 μM of PGT with 500 μM of interfering compounds. (B) Stability of the sensor as its continuous usage for 45 days containing 100 μM PGT in 0.1 M pH 7.0. (C) Plot for reproducibility of WO_3 NBs@GR/GCE containing 100 μM of PGT.

Table 1
Determination of PGT in real samples based on WO_3 NBs@GR/GCE.

Real Samples	Added/nM	Found/nM	Recovery/%	*RSD/%
Blood serum samples 1	100	98.36	98.36	3.59
Blood serum samples 2	200	192.78	96.39	3.12
Blood serum samples 3	300	291.02	97.00	3.36
Blood serum samples 4	400	389.78	97.44	3.19
Blood serum samples 5	500	491.42	98.28	3.36

* Related standard deviation (RSD) of n = 3 independent experiments.

Acknowledgments

Financial assistance received from National Taipei University of Technology is gratefully acknowledged. One of the author Dr. Govindasamy Mani would like to gratitude National Taipei University of technology for the post-doctoral fellowship. The authors (R.J.) extends his appreciation to King Saud University for financial supports through Vice Deanship of Scientific Research Chairs.

Appendix A. Supplementary data

Supplementary data to this article can be found online at https://doi.org/10.1016/j.ultsonch.2019.03.021.

References

[1] A. Gevaerd, S.F. Blaskievicz, A.J. Zarbin, E.S. Orth, M.F. Bergamini, L.H. Marcolino-Junior, Nonenzymatic electrochemical sensor based on imidazole-functionalized graphene oxide for progesterone detection, Biosens. Bioelectron. 112 (2018) 108–113.
[2] V. Serafín, G. Martínez-García, J. Aznar-Poveda, J. Lopez-Pastor, A. Garcia-Sanchez, J. Garcia-Haro, S. Campuzano, P. Yáñez-Sedeño, J. Pingarrón, Determination of progesterone in saliva using an electrochemical immunosensor and a COTS-based portable potentiostat, Anal. Chim. Acta 1049 (2019) 65–73.
[3] M. Arvand, S. Elyan, M.S. Ardaki, Facile one-pot electrochemical synthesis of zirconium oxide decorated poly (3, 4-ethylenedioxythiophene) nanocomposite for the electrocatalytic oxidation and detection of progesterone, Sens. Actuat. B 281 (2019) 157–167.
[4] J.G. Pacheco, P. Rebelo, M. Freitas, H.P. Nouws, C. Delerue-Matos, Breast cancer biomarker (HER2-ECD) detection using a molecularly imprinted electrochemical sensor, Sens. Actuat. B 273 (2018) 1008–1014.
[5] Y. Huang, H. Xiao, Y. Liu, J. Gan, Q. Yan, Column selection approach for related substances determination of progesterone by high-performance liquid chromatography, Chem. Biol. Drug Des. 93 (2019) 29–37.
[6] Y. Wang, A. Partridge, Y. Wu, Improving nanoparticle-enhanced surface plasmon resonance detection of small molecules by reducing steric hindrance via molecular linkers, Talanta (2019).
[7] T. Fehér, K. Fehér, L. Bodrogi, A simple gas-liquid chromatographic method with electron capture detection for the determination of progesterone in the blood of humans and domestic animals, J. Chromatogr. A 111 (1975) 125–132.
[8] I.F. Sommerville, M.T. Pickett, W.P. Collins, D.C. Denyer, A modified method for the quantitative determination of progesterone in human plasma, Eur. J. Endocrinol. 43 (1963) 101–109.
[9] Z. Wu, C. Zhang, C. Yang, X. Zhang, E. Wu, Simultaneous quantitative determination of norgestrel and progesterone in human serum by high-performance liquid chromatography-tandem mass spectrometry with atmospheric pressure chemical ionization, Analyst 125 (2000) 2201–2205.
[10] A. Moore, S. Spahr, Activity monitoring and an enzyme immunoassay for milk progesterone to aid in the detection of estrus, J. Dairy Sci. 74 (1991) 3857–3862.
[11] R. Wehner, A. Handke, Simple and rapid method for the determination of progesterone in rat plasma by gas–liquid chromatography with electron-capture detection, J. Chromatogr. A 177 (1979) 237–244.
[12] H. Wyman, I.F. Sommerville, The description and evaluation of a simple technique for the determination of plasma progesterone by thin-layer and gas-liquid chromatography, Steroids 12 (1968) 63–86.
[13] V. Mani, A.P. Periasamy, S.-M. Chen, Highly selective amperometric nitrite sensor based on chemically reduced graphene oxide modified electrode, Electrochem. Commun. 17 (2012) 75–78.
[14] R. Devasenathipathy, V. Mani, S.-M. Chen, Highly selective amperometric sensor for the trace level detection of hydrazine at bismuth nanoparticles decorated graphene nanosheets modified electrode, Talanta 124 (2014) 43–51.
[15] M. Govindasamy, S.-M. Chen, V. Mani, R. Devasenathipathy, R. Umamaheswari, K.J. Santhanaraj, A. Sathiyan, Molybdenum disulfide nanosheets coated multi-walled carbon nanotubes composite for highly sensitive determination of chloramphenicol in food samples milk, honey and powdered milk, J. Colloid Interface Sci. 485 (2017) 129–136.
[16] M. Govindasamy, V. Mani, S.-M. Chen, T.-W. Chen, A.K. Sundramoorthy, Methyl parathion detection in vegetables and fruits using silver@ graphene nanoribbons nanocomposite modified screen printed electrode, Sci. Rep. 7 (2017) 46471.
[17] U. Rajaji, M. Govindasamy, S.-M. Chen, T.-W. Chen, X. Liu, S. Chinnapaiyan, Microwave-assisted synthesis of Bi_2WO_6 flowers decorated graphene nanoribbon composite for electrocatalytic sensing of hazardous dihydroxybenzene isomers, Compos. B Eng. 152 (2018) 220–230.
[18] M. Govindasamy, U. Rajaji, S.-M. Chen, S. Kumaravel, T.-W. Chen, F.M. Al-Hemaid, M.A. Ali, M.S. Elshikh, Detection of pesticide residues (Fenitrothion) in fruit samples based on niobium carbide@ molybdenum nanocomposite: an electrocatalytic approach, Anal. Chim. Acta 1030 (2018) 52–60.
[19] D. Meng, T. Yamazaki, Y. Shen, Z. Liu, T. Kikuta, Preparation of WO_3 nanoparticles and application to NO_2 sensor, Appl. Surf. Sci. 256 (2009) 1050–1053.
[20] S. Li, I.N. Germanenko, M.S. El-Shall, Semiconductor nanoparticles in contact: quenching of the photoluminescence from silicon nanocrystals by WO_3 nanoparticles suspended in solution, J. Phys. Chem. B 102 (1998) 7319–7322.
[21] L. Wang, A. Teleki, S.E. Pratsinis, P. Gouma, Ferroelectric WO_3 nanoparticles for acetone selective detection, Chem. Mater. 20 (2008) 4794–4796.
[22] S.H. Lee, R. Deshpande, P.A. Parilla, K.M. Jones, B. To, A.H. Mahan, A.C. Dillon, Crystalline WO_3 nanoparticles for highly improved electrochromic applications, Adv. Mater. 18 (2006) 763–766.
[23] R. Ganesan, A. Gedanken, Synthesis of WO_3 nanoparticles using a biopolymer as a template for electrocatalytic hydrogen evolution, Nanotechnology 19 (2007) 025702.
[24] A. Anithaa, N. Lavanya, K. Asokan, C. Sekar, WO_3 nanoparticles based direct electrochemical dopamine sensor in the presence of ascorbic acid, Electrochim. Acta 167 (2015) 294–302.
[25] V. Hariharan, S. Radhakrishnan, M. Parthibavarman, R. Dhilipkumar, C. Sekar, Synthesis of polyethylene glycol (PEG) assisted tungsten oxide (WO_3) nanoparticles for L-dopa bio-sensing applications, Talanta 85 (2011) 2166–2174.
[26] K.K. Akurati, A. Vital, J.-P. Dellemann, K. Michalow, T. Graule, D. Ferri, A. Baiker, Flame-made WO_3/TiO_2 nanoparticles: relation between surface acidity, structure

and photocatalytic activity, Appl. Catal. B 79 (2008) 53–62.
[27] N. Jeromiyas, E. Elaiyappillai, A.S. Kumar, S.-T. Huang, V. Mani, Bismuth nanoparticles decorated graphenated carbon nanotubes modified screen-printed electrode for mercury detection, J. Taiwan Inst. Chem. Eng. 95 (2019) 466–474.
[28] M. Govindasamy, S.-F. Wang, S. Kumaravel, R.J. Ramalingam, H.A. Al-lohedan, Facile synthesis of copper sulfide decorated reduced graphene oxide nanocomposite for high sensitive detection of toxic antibiotic in milk, Ultrason. Sonochem. (2018).
[29] S. Manavalan, U. Rajaji, S.-M. Chen, S.S.P. Selvin, M. Govindasamy, T.-W. Chen, M.A. Ali, F.M. Al-Hemaid, M. Elshikh, Determination of 8-hydroxy-2′-deoxyguanosine oxidative stress biomarker using dysprosium oxide nanoparticles@ reduced graphene oxide, Inorg. Chem. Front. 5 (2018) 2885–2892.
[30] M. Govindasamy, S. Sakthinathan, S.M. Chen, T.W. Chiu, A. Sathiyan, J.P. Merlin, Reduced graphene oxide supported cobalt Bipyridyl complex for sensitive detection of methyl parathion in fruits and vegetables, Electroanalysis 29 (2017) 1950–1960.
[31] V. Mani, M. Govindasamy, S.-M. Chen, T.-W. Chen, A.S. Kumar, S.-T. Huang, Core-shell heterostructured multiwalled carbon nanotubes@ reduced graphene oxide nanoribbons/chitosan, a robust nanobiocomposite for enzymatic biosensing of hydrogen peroxide and nitrite, Sci. Rep. 7 (2017) 11910.
[32] S. Kogularasu, M. Govindasamy, S.-M. Chen, M. Akilarasan, V. Mani, 3D graphene oxide-cobalt oxide polyhedrons for highly sensitive non-enzymatic electrochemical determination of hydrogen peroxide, Sens. Actuat. B 253 (2017) 773–783.
[33] V. Mani, M. Govindasamy, S.-M. Chen, B. Subramani, A. Sathiyan, J.P. Merlin, Determination of folic acid using graphene/molybdenum disulfide nanosheets/gold nanoparticles ternary composite, Int. J. Electrochem. Sci. 12 (2017) e267.
[34] M. Govindasamy, V. Mani, S.-M. Chen, T. Maiyalagan, S. Selvaraj, T.-W. Chen, S.-Y. Lee, W.-H. Chang, Highly sensitive determination of non-steroidal anti-inflammatory drug nimesulide using electrochemically reduced graphene oxide nanoribbons, RSC Adv. 7 (2017) 33043–33051.
[35] M. Govindasamy, R. Umamaheswari, S.-M. Chen, V. Mani, C. Su, Graphene oxide nanoribbons film modified screen-printed carbon electrode for real-time detection of methyl parathion in food samples, J. Electrochem. Soc. 164 (2017) B403–B408.
[36] Y. Hou, F. Zuo, A.P. Dagg, J. Liu, P. Feng, Branched WO_3 nanosheet array with layered C_3N_4 heterojunctions and CoO_x nanoparticles as a flexible photoanode for efficient photoelectrochemical water oxidation, Adv. Mater. 26 (2014) 5043–5049.
[37] N. Huo, Q. Yue, J. Yang, S. Yang, J. Li, Abnormal photocurrent response and enhanced photocatalytic activity induced by charge transfer between WS_2 nanosheets and WO_3 nanoparticles, ChemPhysChem 14 (2013) 4069–4073.
[38] L. Santos, C.M. Silveira, E. Elangovan, J.P. Neto, D. Nunes, L. Pereira, R. Martins, J. Viegas, J.J. Moura, S. Todorovic, Synthesis of WO_3 nanoparticles for biosensing applications, Sens. Actuat. B 223 (2016) 186–194.
[39] B. Unnikrishnan, V. Mani, S.-M. Chen, Highly sensitive amperometric sensor for carbamazepine determination based on electrochemically reduced graphene oxide–single-walled carbon nanotube composite film, Sens. Actuat. B 173 (2012) 274–280.
[40] V. Mani, R. Devasenathipathy, S.-M. Chen, S.-F. Wang, P. Devi, Y. Tai, Electrodeposition of copper nanoparticles using pectin scaffold at graphene nanosheets for electrochemical sensing of glucose and hydrogen peroxide, Electrochim. Acta 176 (2015) 804–810.
[41] M. Govindasamy, S.-M. Chen, V. Mani, M. Akilarasan, S. Kogularasu, B. Subramani, Nanocomposites composed of layered molybdenum disulfide and graphene for highly sensitive amperometric determination of methyl parathion, Microchim. Acta 184 (2017) 725–733.
[42] N.-H. Kim, S.-J. Choi, S.-J. Kim, H.-J. Cho, J.-S. Jang, W.-T. Koo, M. Kim, I.-D. Kim, Highly sensitive and selective acetone sensing performance of WO_3 nanofibers functionalized by Rh_2O_3 nanoparticles, Sens. Actuat. B 224 (2016) 185–192.
[43] A. Hoel, L. Reyes, S. Saukko, P. Heszler, V. Lantto, C. Granqvist, Gas sensing with films of nanocrystalline WO_3 and Pd made by advanced reactive gas deposition, Sens. Actuat. B 105 (2005) 283–289.
[44] Z. Zhang, X. Wang, Z. Cui, C. Liu, T. Lu, W. Xing, Pd nanoparticles supported on WO_3/C hybrid material as catalyst for oxygen reduction reaction, J. Power Sources 185 (2008) 941–945.
[45] P.-G. Su, S.-L. Peng, Fabrication and NO_2 gas-sensing properties of reduced graphene oxide/WO3 nanocomposite films, Talanta 132 (2015) 398–405.
[46] B. Weng, J. Wu, N. Zhang, Y.-J. Xu, Observing the role of graphene in boosting the two-electron reduction of oxygen in graphene–WO_3 nanorod photocatalysts, Langmuir 30 (2014) 5574–5584.
[47] X. Jie, D. Zeng, J. Zhang, K. Xu, J. Wu, B. Zhu, C. Xie, Graphene-wrapped WO_3 nanospheres with room-temperature NO_2 sensing induced by interface charge transfer, Sens. Actuat. B 220 (2015) 201–209.
[48] D. Shao, M. Yu, J. Lian, S. Sawyer, An ultraviolet photodetector fabricated from WO_3 nanodiscs/reduced graphene oxide composite material, Nanotechnology 24 (2013) 295701.
[49] M. Govindasamy, S. Shanthi, E. Elaiyappillai, S.-F. Wang, P.M. Johnson, H. Ikeda, Y. Hayakawa, S. Ponnusamy, C. Muthamizhchelvan, Fabrication of hierarchical $NiCo_2S_4$@CoS_2 nanostructures on highly conductive flexible carbon cloth substrate as a hybrid electrode material for supercapacitors with enhanced electrochemical performance, Electrochim. Acta 293 (2019) 328–337.
[50] U. Rajaji, S. Manavalan, S.-M. Chen, M. Govindasamy, T.-W. Chen, T. Maiyalagan, Microwave-assisted synthesis of europium (III) oxide decorated reduced graphene oxide nanocomposite for detection of chloramphenicol in food samples, Compos. B Eng. 161 (2019) 29–36.
[51] J. Di, J. Xia, Y. Ge, H. Li, H. Ji, H. Xu, Q. Zhang, H. Li, M. Li, Novel visible-light-driven CQDs/Bi_2WO_6 hybrid materials with enhanced photocatalytic activity toward organic pollutants degradation and mechanism insight, Appl. Catal. B 168 (2015) 51–61.
[52] Y. Huang, S. Kang, Y. Yang, H. Qin, Z. Ni, S. Yang, X. Li, Facile synthesis of Bi/Bi_2WO_6 nanocomposite with enhanced photocatalytic activity under visible light, Appl. Catal. B 196 (2016) 89–99.
[53] C. Li, G. Chen, J. Sun, Y. Feng, J. Liu, H. Dong, Ultrathin nanoflakes constructed erythrocyte-like Bi_2WO_6 hierarchical architecture via anionic self-regulation strategy for improving photocatalytic activity and gas-sensing property, Appl. Catal. B 163 (2015) 415–423.